Bioconjugate Chemistry

Article

pubs.acs.org/bc

Design Considerations for RNA Spherical Nucleic Acids (SNAs)

Stacey N. Barnaby,[†,‡] Grant A. Perelman,[†,‡] Kevin L. Kohlstedt,[†] Alyssa B. Chinen,[†,‡] George C. Schatz,[†,‡] and Chad A. Mirkin*[,†,‡]

[†]Department of Chemistry and [‡]International Institute for Nanotechnology, Northwestern University, 2145 Sheridan Road, Evanston, Illinois 60208, United States

Supporting Information

ABSTRACT: Ribonucleic acids (RNAs) are key components in many cellular processes such as cell division, differentiation, growth, aging, and death. RNA spherical nucleic acids (RNA-SNAs), which consist of dense shells of double-stranded RNA on nanoparticle surfaces, are powerful and promising therapeutic modalities because they confer advantages over linear RNA such as high cellular uptake and enhanced stability. Due to their three-dimensional shell of oligonucleotides, SNAs, in comparison to linear nucleic acids, interact with the biological environment in unique ways. Herein, the modularity of the RNA-SNA is used to systematically study structure−function relationships in order to understand how the oligonucleotide shell affects interactions with a specific type of biological environment, namely, one that contains serum nucleases. We use a combination of experiment and theory to determine the key architectural properties (i.e., sequence, density, spacer moiety, and backfill molecule) that affect how RNA-SNAs interact with serum nucleases. These data establish a set of design parameters for SNA architectures that are optimized in terms of stability.

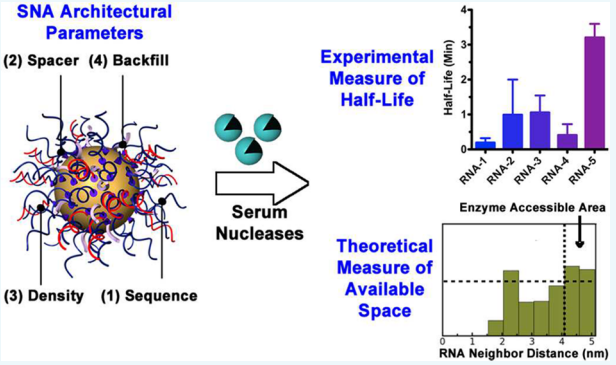

INTRODUCTION

Spherical nucleic acids (SNAs) are an emerging class of nanomaterials that consist of nanoparticle cores densely functionalized with shells of oriented oligonucleotides.[1] SNAs are promising single-entity constructs capable of actively moving into cells and effecting nucleic acid-dependent processes without triggering an unwanted immune response.[2,3] Consequently, they have become the basis for hundreds of biological and medical tools.[4−7] RNA-SNAs are of particular interest because of their potential to significantly impact the field of medicine in areas such as gene regulation, immune modulation, and cancer therapy.[8,9] For example, SNAs comprising small interfering RNA (siRNA) are promising agents for treating glioblastoma multiforme[10] and diabetic wounds[11] in animal models. In the former case, treatment strategies take advantage of the ability of SNAs to cross the blood-brain-barrier, and in the latter case, they take advantage of the unusual ability of SNAs to penetrate the skin.

Due to their three-dimensional presentation and orientation of oligonucleotides, the interaction of SNA oligonucleotide shells with biological environments (i.e., cell surface receptors, enzymes, proteins) is fundamentally different than what is observed for conventional linear forms of nucleic acids[12−16] (linear used here in contrast to spherical nucleic acids, but not taking into account possible secondary structure). For example, SNAs, despite their negative charge, readily enter most cells (except red blood cells)[17] without triggering an innate immune response,[3] whereas conventional forms of nucleic acids require transfection agents, which often stimulate an unwanted immune response, in order to enter cells.[18−20] It has been shown that the rapid cellular uptake kinetics and intracellular delivery of SNAs is an active process that is often dependent on class A scavenger receptors, which recognize the high-density spherical arrangement of oligonucleotides and to which the SNAs bind with high affinity.[12,13,21,22] In contrast, oligonucleotides complexed with positively charged transfection reagents enter cells through an electrostatic interaction with the plasma membrane and subsequently enter cells most commonly through membrane destabilization.[23−26]

Despite the advances using siRNA-SNAs in medicine, how such structures interact with biological enzymes is poorly understood. This process is fundamentally important, because in order for the RNA to perform its designated tasks *in vitro* and *in vivo*, interactions between the RNA and specific enzymes are essential. For example, there is a delicate balance between evading the enzymes that cause nuclease-catalyzed hydrolysis of RNA while simultaneously allowing enzymatic recognition of RNA so that it can perform its designated function.[27] For conventional forms of RNA, it is known that RNase A type enzymes play a role in the nuclease-catalyzed hydrolysis of RNA, specifically at 5′-3′/3′-5′ UA/AU motifs.[28−31] Due to the high density of oligonucleotides in a spherical arrangement and the unique interactions of oligonucleotides with biological enzymes and proteins, we sought to determine whether RNA-

Received: June 28, 2016
Revised: July 21, 2016
Published: August 14, 2016

DOI: 10.1021/acs.bioconjchem.6b00350
Bioconjugate Chem. 2016, 27, 2124−2131

SNAs, as a class of oligonucleotides, are similarly degraded by these types of enzymes. Significantly, despite their seemingly dense structure, we discovered that nucleases could access SNAs at sites near the surface of the particle core. This observation led us to ask how macromolecules, such as enzymes, are able to move in and out of the SNA architecture. A combination of fluorescence-based assays, designed to probe structure, as well as molecular dynamics (MD) simulations were used to answer this question. Collectively, these data establish the following three design considerations for synthesizing stable and active SNAs: (1) If one desires RNA to remain on the nanoparticle surface, avoid motifs of UA/AU close to the gold nanoparticle (AuNP) surface. (2) Spacer units, typically composed of hexaethylene glycol or DNA, can be used to optimize oligonucleotide presentation and to control distance from the AuNP core. (3) Increased nucleic acid density retards serum nuclease activity.

RESULTS AND DISCUSSION

Design of RNA Spherical Nucleic Acid (RNA-SNA) Nanoparticle Conjugates. RNA-SNAs are typically composed of three key components: (1) a nanoparticle core; (2) an RNA duplex; and (3) often backfill molecules for passivating the unmodified nanoparticle surface and stabilizing the SNA structure (Figure 1).[10,11,14,15,32] From a gene-regulation standpoint, since many of the properties of SNAs arise from the dense shell of oligonucleotides,[21,33] the chemical identity of the core is not critical. Therefore, for this study, we have chosen to work with 13 nm gold nanoparticles since, thus far, they are the most studied and extensively utilized nanoparticle core for RNA-SNAs.[10,11,15,32] siRNA duplexes, each containing one oligonucleotide with a propylthiol group, were used as the adsorbates to synthesize the SNA architecture. The propylthiol group was chosen because it readily adsorbs onto gold and the precursors to prepare it are commercially available. The RNA duplex also contains a spacer region, typically an oligoethylene glycol spacer ($[(C_2H_4O)_6\text{-}PO_3^-]_2$; Sp2), that serves to separate the recognition sequence from the nanoparticle surface. Unless specified otherwise, two oligoethylene glycol spacers were used (Sp2). The actual RNA sequence is then chosen based on the intended application. Specifically for gene knockdown, one strand of the siRNA duplex (the antisense (AS) strand) is complementary to the mRNA (mRNA) of interest. Finally, backfill molecules consisting of (11-mercaptoundecyl)tetra(ethylene glycol) (OEG)[15] or a thiolated polyethylene glycol (PEG)[14] are typically used to passivate remaining gold sites to increase the colloidal stability of the siRNA-SNAs (SI Discussion 1.1).

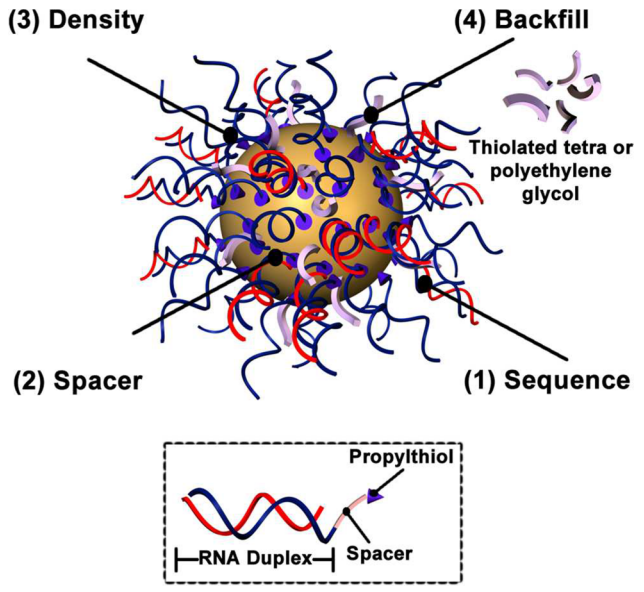

Figure 1. Design parameters studied for RNA-SNAs. RNA-SNAs are typically synthesized from three components: a thiol-modified RNA duplex, a nanoparticle core, and a backfill molecule. The SNAs are highly modular in that each of these components can be fine-tuned to meet the desired need of the SNA.

Although each of these three components is necessary for the successful implementation of RNA-SNAs, the relative importance of each in the design of stable and active RNA-SNAs for gene regulation is not known. Of specific interest are the parameters that lead to functional and potent siRNA gene knockdown and construct stability, two properties that are intimately related. Indeed, it is known that foreign nucleic acids are degraded by serum nucleases,[34] and to be functional as gene knockdown agents, SNAs must avoid such enzymes so that they can specifically engage with the RNA interference (RNAi) machinery. In the subsequent sections, we study each of these SNA components in an effort to determine which parameters influence nuclease recognition and degradation of this class of constructs.

Design Parameter 1: Sequence. In practice, any desired RNA sequence can be synthesized and functionalized on the surface of an SNA, depending on the desired application, and thus there is a near-infinite number of RNA sequences and SNAs that can be synthesized. Previous reports looking at the interaction of enzymes with two different RNA-SNAs, as well as conventional linear forms of RNA, suggest that sequence plays a large role in how serum nucleases interact with RNA.[14,15,30] We conducted a systematic study with ten different SNAs, each synthesized with a unique RNA sequence (Table S1, Figures S1, S2) to determine how sequence affects RNA−enzyme interactions when the RNA is oriented on nanoparticle surfaces. The interaction of each SNA with serum nucleases in the form of 10% fetal bovine serum (FBS) was studied as a model system for RNA-SNA-enzyme interactions (Figure 2a and Figure S3). The AS RNA half-lives were measured to be highly sequence dependent (Figure 2b), which is in agreement with results for particle-free RNA.[30] The stabilities of linear duplexes of sequence-1 and sequence-7 were measured, and the same trend in stability of the RNA-SNAs was observed (Figure S4). Thus, these data further illustrate that each SNA is a unique chemical entity, as manifested by the observation that the RNA sequence is pivotal in dictating the rate at which enzymatic hydrolysis occurs.

We then analyzed a subset of the data in Figure 2b to determine the characteristic of the sequence that was the most significant determinant in the half-life of the RNA on the nanoparticle surface. The base composition of the sequence was kept constant, but the position of different components of the sequence was systematically changed. For this study, we compared SNAs 4−6, which are variants of SNA-3.[14] Specifically, sequence-3 was divided into four different sections (designated as "blocks"), which were then systematically moved one "block" away from the nanoparticle surface (Figure 2c and SI Discussion 1.2). Despite the fact that the same nucleobases were present in all four sequences, the proximity of different

DOI: 10.1021/acs.bioconjchem.6b00350
Bioconjugate Chem. 2016, 27, 2124−2131

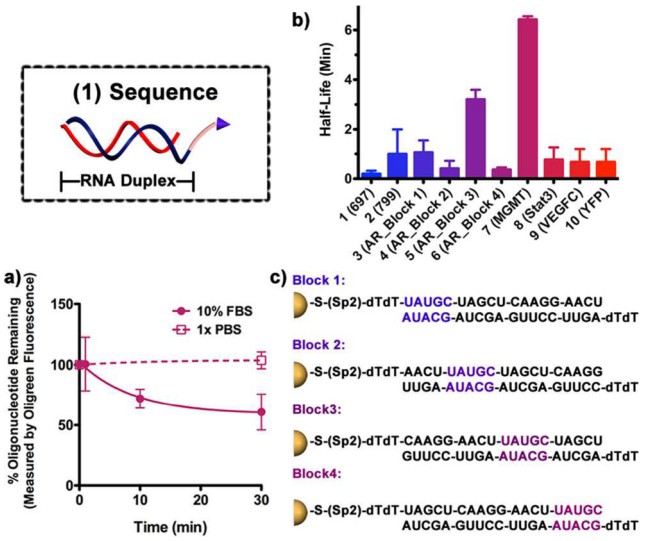

Figure 2. Effect of sequence on the rate of nuclease-catalyzed hydrolysis of RNA-SNAs. (a) Sample data set for measuring the interaction of RNA-SNAs with enzymes. Here, a plot of % oligonucleotide remaining versus time for sequence-7 (MGMT) in 10% fetal bovine serum (FBS; circle) and 1× phosphate buffered saline (PBS; open square) is shown. The data points for 10% FBS were fit to a first-order decay function and the data points for 1× PBS were fit to a linear regression. (b) A data set like the one in (a) was generated for the 10 different RNA-SNAs with sequences written in Table S1. From the first-order decay function, half-lives were calculated and plotted, where the error bars represent standard deviation in half-life for $n = 3$ biological replicates. (c) Sequences 3–6 were generated by taking sequence-3 (Androgen receptor; AR_Block 1) and dividing it into four sections (or "blocks"). The first five nucleotides are then moved systematically farther away from the nanoparticle surface. As shown in (a), the order of the blocks has a dramatic effect on the stability and half-life of the RNA.

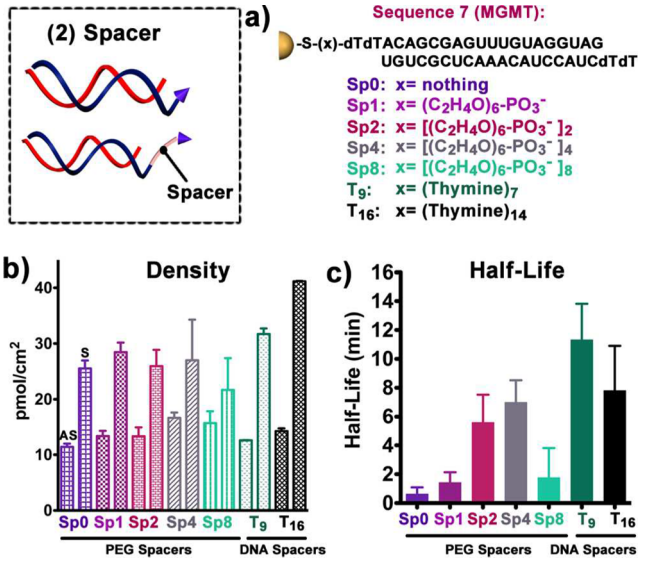

Figure 3. How spacer unit affects the stability of RNA-SNAs. (a) The number of spacer units between the propyl thiol group and the recognition sequence was altered systematically. (b) Oligonucleotide density, within error, is kept constant despite changes in the identity of the spacer moiety. (c) The half-life of the oligonucleotide on the nanoparticle increases with increasing number of hexaethylene glycol spacer units up to Sp4, before decreasing. SNAs with a T_{16} spacer exhibited similar stability as their size counterpart Sp4, whereas SNAs with a T_9 spacer had the greatest stability observed. Error bars represent the standard deviation for $n = 3$ biological replicates.

blocks (or more specifically, motifs) to the nanoparticle surface greatly affected the RNA half-life in serum nucleases (Figure 2c). The sequences with U-A motifs closest to the nanoparticle surface (sequence-3 (named Block 1) and sequence-6 (named Block 4)) showed the fastest rate of nuclease-catalyzed hydrolysis ($\tau_{1/2} < 1$ min). These data, as well as the data for SNAs-1,2,8,9 (Figure 2b) suggest that this motif, when close to the nanoparticle surface, is rapidly hydrolyzed by serum nucleases and is consistent with results for linear siRNA duplexes.[29] Despite the fact that the SNA architecture consists of a densely packed, oriented array of RNA oligonucleotides, sequences with motifs recognized by RNases are rapidly degraded, similar to conventional nucleic acids.[28−31] This led to design parameter 1, for retaining RNA on the nanoparticle surface: avoid motifs of UA/AU close to the gold nanoparticle (AuNP) surface. This observation begs the question—how do we think about the SNA architecture and types of macromolecules that are able to move in and out of the SNA structure? The desire to understand the space available for macromolecules to approach the nanoparticle surface led us to explore the next design parameter.

Design Parameter 2: Spacer Region. The next design parameter explored was the spacer region, which is defined as the distance between the propyl thiol group and the RNA recognition sequence (Figure 3a). Previous reports for DNA-SNAs have studied how the spacer region affects the oligonucleotide loading,[35] and thus we chose the two highest density spacer motifs: hexaethylene glycol and polythymine DNA (polyT). Seven different thiolated sense oligonucleotides were synthesized with varying numbers of hexaethylene glycol spacer units ((Spx; $(C_2H_4O)_6$-$PO_3^-)_x$), where $x = 0$, 1, 2, 4, and 8) as well as different numbers of polyT DNA (T_9 and T_{16}; Figure 3a) and subsequently functionalized on the surface of 13 nm gold nanoparticles (Figure S1b). The sense and AS oligonucleotide densities were measured and found to be comparable irrespective of the spacer identity (Figure 3b).

An increase in the diameter of the SNAs was observed by dynamic light scattering as the spacer region was increased from Sp0 (22.29 nm ± 1.1) to Sp8 (32.28 nm ± 1.58), thus suggesting that each spacer unit adds ∼1.25 nm to the overall SNA diameter, as opposed to the theoretical length of 3 nm for a fully stretched hexaethylene glycol chain with phosphate group[36] (Figure S5a). This is consistent with observations for nanoparticles functionalized with DNA using different numbers of hexaethylene glycol spacers, where the spacer was coiled in its equilibrium position on the surface of the nanoparticle.[36] For SNAs with polyT spacers, an increase in hydrodynamic diameter was also observed (Figure S5a).

We then sought to determine if changing the distance of the recognition sequence from the nanoparticle surface had any effect on serum nucleases accessing the oligonucleotide shell. SNA-7 (MGMT) was used for this study for two reasons: (1) the measured half-life in 10% FBS is the longest of the ten sequences studied (Figure 2b), and (2) the sequence has exhibited potent gene knockdown previously *in vitro* and in an animal model.[37] RNA-SNAs with Sp0 and Sp1 exhibited very rapid interactions with serum nucleases, whereas subsequently slower cleavage and thus longer half-life of the AS oligonucleotide on the nanoparticle surface was observed for Sp2 and Sp4, before decreasing again for Spx, when $x > 4$

DOI: 10.1021/acs.bioconjchem.6b00350
Bioconjugate Chem. 2016, 27, 2124−2131

(Figure 3c, Figure S5b). While SNA-7 with a T_{16} spacer exhibited similar rates of nuclease-catalyzed hydrolysis as the similarly sized Sp4, SNA-7 with a T_9 spacer exhibited the slowest rate of hydrolysis (Figure 3c, Figure S5b). These data show that when polyT DNA serves as the spacer region this slows down the rate of nuclease-catalyzed hydrolysis, which we speculate is, in part, due to the charged, stiff DNA spacer, which pushes the recognition sequence away from the nanoparticle surface compared to the more flexible hexaethylene glycol spacers.

Thus far, we have seen that serum nucleases are able to deeply penetrate the SNA architecture and changing the distance of the recognition sequence from the nanoparticle surface changes the rate of serum nuclease hydrolysis. In order to measure how the spacer units affect the ability of the enzyme to access regions of RNA that appear shielded, we turned to coarse-grained (CG) MD simulations to measure the radius of gyration of RNA as a function of the number of spacers for RNA-SNAs (Figure 4). We based our CG RNA model on a

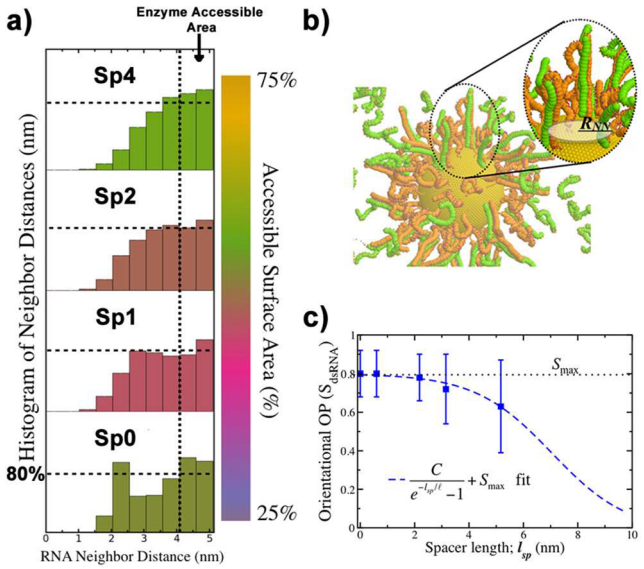

Figure 4. Molecular dynamics structural analysis of RNA-SNAs. (a) Set of nearest-neighbor distance histograms (normalized) for four SNA spacer lengths. The color bar represents the percentage of surface accessible area for a model spherical RNase. The vertical dashed line represents the smallest distance required for an enzyme to reach nucleotides at the 5′ end of the AS oligonucleotide (end near AuNP surface). The horizontal dashed line is a guide for the eye, where the distance probability is greater than 80% of the maximum value at 4.05 nm for Sp0. The line is at the same value for the other spacer lengths. (b) MD snapshot of RNA-SNA with Sp1, where free complementary RNA oligonucleotides are green and tethered RNA is brown. Inset shows the nearest-neighbor search radius R_{NN}, which was calculated around all dsRNA at the 5′ end. (c) SNA orientational order parameter S, calculated for dsRNA on the SNA and ensemble averaged over the MD trajectories for four spacer lengths. Dashed fit shows a sigmoidal decay with a proportionality constant C = 0.82, decay length = 1.41 nm, and S_{max} = 0.80.

previous model that described the hybridization thermodynamics of DNA on nanoparticle surfaces.[38] The basis of the CG RNA model is taken from a discrete worm-like chain (WLC) model with the RNA elastic properties being derived from the electrostatic repulsion of the negatively charged backbone and its intrinsic bending stiffness (SI Discussion 1.3).[39] The discretization of the CG RNA model is a "one bead per base" scheme and is constructed on top of a model 13 nm Au spherical shell with the CG RNA strands tethered to random sites on the sphere. Electroneutrality is preserved via sodium (Na^+) counterions, and the bulk salt concentration is controlled by $[Na^+][Cl^-]$ ions. We can control the degree of hybridization for the RNA-SNAs via CG complement RNA strands that are free to hybridize/dehybridize with the tethered strands and we can monitor the percentage of double-stranded RNA on the SNA by tracking the bonding state of each bead.[40] In order to mimic the addition of hexaethylene glycol spacers, the number of small elastic beads can be altered to control the length of the spacer. To mimic experimental conditions, MD trajectories were run for 40% SNA hybridization, and the RNA structural properties were analyzed as a function of spacer length. We first looked at the elastic properties of the model RNA by computing the radius of gyration components (r, Θ, ϕ) of each strand (R_G; SI Discussion 1.4). Considering the difference between no spacer (Sp0) and Sp1, we found that the ssRNA becomes stiffer when the spacer length is shortened from Sp1 to Sp0 since the average R_G per ssRNA goes from 1.28 ± 0.14 nm to 1.46 ± 0.15 nm, respectively (Figures S6, S7). For longer spacers, we observed little difference in the length, and these data show that the R_G per ssRNA does not statistically change going to longer spacer lengths (Sp2, Sp4), suggesting that the ssRNA does not feel a significant reduction in the repulsion or tension in the SNA at spacer lengths longer than Sp4. Additionally, we calculated the R_G of dsRNA and found that the duplexed strands' R_G remains invariant to spacer length (Figure S8), which is consistent with the Sp1 observation for DNA-SNAs (Figure S9).[38] Therefore, we focused on the unhybridized strands because the R_G of the unhybridized strands is more sensitive to different spacer lengths. We note however that the orientation mobility and alignment do not follow the same trends, as dsRNAs gain additional rotational degrees of freedom with longer spacers (see Figure S10; SI discussion 1.4).

The change in the overall structure of the RNA with different spacers affects more than just the length of the RNA oligonucleotides, because as the stiffness of the RNA changes so does the available space between the RNA strands. To measure the distance between neighboring RNA oligonucleotides, we calculated the nearest-neighbor distances between the RNA and related the distances to a set of normalized histograms (Figure 4a). This calculation used a search radius (R_{NN}) centered over the 3′ sense oligonucleotide of the dsRNA so as to not double count (see Figures 4b and S10 for SNA visualization). However, at longer spacer lengths, the neighbor search was expanded to the 5′ end of the sense oligonucleotide (i.e., the end away from the nanoparticle surface). This was necessary since the RNA oligonucleotides were no longer consistently splaying normal to the surface of the AuNP core when the flexible spacer was longer than 3 nm or greater than Sp2. Because the closest neighboring nucleotide within R_{NN} was no longer guaranteed to be oriented from the 3′ end, the neighbor search scanned over both ends of the RNA oligonucleotides to find the closest contact. Surprisingly, the histograms in Figure 4a show that SNAs with either the smallest or larger number of spacers (Sp0 and Sp4, respectively) have the greatest amount of accessible free-volume (area to right of vertical dash in Figure 4a) despite the fact that the RNA oligonucleotides with Sp0 are closest to the AuNP core. This is due in part to the radial elastic repulsion

DOI: 10.1021/acs.bioconjchem.6b00350
Bioconjugate Chem. 2016, 27, 2124−2131

that the RNA oligonucleotides feel (described above) as well as the orientational alignment of the dsRNA (Figure 4c). This leads to a bimodal distribution of close nearest neighbors (<4 nm) and farther nearest neighbors (>4 nm) relative to the size of ribonuclease (RNase) A (unit cell parameters (in nm): a = 3.66, b = 4.05, c = 5.23).[41] For longer spacers, the SNA nearest-neighbor distributions in Figure 4a become more uniform, but do not show a centered distribution above the RNase spherical model size of 4.05 nm until Sp4 and larger. Additionally, we calculated the orientational alignment of the dsRNA on the SNA to show the effect of the spacer on the directional order of the dsRNA. Because the rotational degrees of freedom of the RNA change with the spacer length, a nematic order parameter (S) based on the departure angle of the dsRNA to the normal vector of the surface of the AuNP is used (Figure 4c; see SI for details). We fit S to a sigmoidal curve that has a decay constant of l = 1.41 nm and maximum S_{max} = 0.8. In Figure 4c the order parameter S decays to 0 (i.e., no orientational order) when the spacer length (l_{sp}) becomes larger than the size of the gold core (~13 nm). The model may provide guidance as to why UA/AU motifs away from the AuNP surface are longer-lived. Although this model does not capture secondary structure, it does recover the known behavior of the terminal bases switching between hybridized and unhybridized states due to entropic effects such as end fraying.[42] Floppy motifs may be behind the increase in half-life for SNA-7 due to the enzyme being forced to wait in order to bind to the RNA. The RNA-SNA structural analysis of the MD trajectories suggests that the spacer length can be a critical design parameter to modulate the available space, and the subsequent rate of enzymatic hydrolysis, on the nanoparticle surface.

The RNA-SNA structural predictions, taken from the MD data, are consistent with our previous hypothesis for RNase A type enzymes causing nuclease-catalyzed hydrolysis of RNA-SNAs[14] and confirm that there is volume available at the nanoparticle surface to accommodate enzymes of this size. This leads to design parameter 2, where the spacer region is used to optimize oligonucleotide presentation and to control the distance from the AuNP core. Specifically, *both experimental and computational studies corroborate that intermediate spacer regimes* (Spx, where $x \geq 1$ and ≤ 4) *are where the surface-immobilized RNA is most stable*. We find that the two SNAs with the slowest rate of nuclease-catalyzed hydrolysis, SNA-5 and SNA-7 (Figure 2b), were the only two SNAs lacking 5′-3′/3′-5′ motifs of UA/AU close to the nanoparticle surface (<7 nucleotides; Table S1), which is the primary motif recognized by RNase A.[28−31] It has also been observed that the purified enzyme interacts with SNAs in a similar manner to 10% FBS (Figure S11). These data demonstrate how the orientation and presentation of the oligonucleotide shell dictates the response to serum nucleases, which leads us to study the next design parameter.

Design Parameter 3: Density. It has been observed previously that changing the density of duplexes on a DNA-SNA did not change the rate of degradation in solutions of DNase 1.[16] Thus, we wanted to investigate whether changes in RNA density would have a similar effect. We synthesized variants of SNA-7 with different densities and ratios of AS:sense oligonucleotides on the surface of the nanoparticle (Figure 5a, Figure S1b). It was observed that interactions between RNA-SNAs and serum nucleases are dependent on the density of the SNA (Figure 5b), as the half-lives of SNA 7−1 and 7−2, with similar densities of AS oligonucleotides, are comparable to one another (Figure 5c) and are the longest observed of any SNA in this study (Figure 5c). For SNA 7−3 (half the density of AS oligonucleotides), the half-life is substantially shorter than that of SNAs 7−1 and 7−2 ($\tau \approx 4$ min versus >12 min), thus further illustrating that *decreasing the number of duplexed oligonucleotides on the nanoparticle surfaces renders the SNA more accessible to enzymes*. The modularity of SNAs thus allows one to keep the sequence the same but change the rate at which enzymes recognize the RNA, which may be useful when endowing SNAs with additional functionality such as being photocleavable[43] or having pH sensitive linkers.[44] It is also worth noting that as the materials design space for SNA cores increases, it is important to retain the high-density architecture of the oligonucleotide shell to confer nuclease stability. The importance of filling free volume on the nanoparticle surface led us to study our final design parameter.

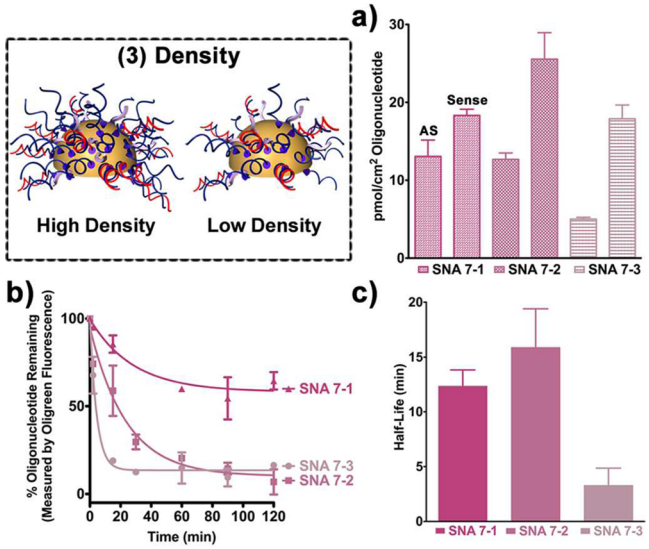

Figure 5. Effect of density on the stability of RNA-SNAs. (a) SNA-7 synthesized with different densities of oligonucleotides. SNA 7−1 represents the SNA with the closest ratio of 1:1 sense:AS oligonucleotide achieved. SNA 7−2 represents comparable AS loading to 7−1 but an increase in the density of thiolated sense RNA. SNA 7−3 represents a comparable density of sense oligonucleotides to previous SNAs but a decrease in the AS oligonucleotide loading. Error bars represent n = 4 measurements. (b) Plot of % oligonucleotide remaining on the SNAs versus time. The SNAs were incubated in 10% FBS for 2 h and readings were taken to determine the amount of oligonuleotide remaining on the nanoparticle surface. The experimental data points were fit to a first-order exponential decay function. Error bars represent n = 2 biological replicates for each time point. (c) Plots of the half-lives from the first-order exponential decay function in (b). These data show that the SNAs with the highest density are the most stable structures. Error bars represent the standard deviation between n = 2 biological replicates.

Design Parameter 4: Backfill. When comparing SNA-7−1 to SNA 7, almost identical AS densities were observed, but due to a longer PEG 2K incubation time (72 h versus 6 h, respectively), an increase in half-life was observed ($\tau \approx 13$ min versus 7 min, respectively; Figure 5b,c versus Figure 2a,b). This illustrates the important role of the backfill in passivating the remaining gold surface and decreasing enzymatic access to the oligonucleotides that has previously not been explored. This observation not only leads to the important design parameter (consume as much free volume on the nanoparticle surface with ligands) but also provides insight into the complex

DOI: 10.1021/acs.bioconjchem.6b00350
Bioconjugate Chem. 2016, 27, 2124−2131

structure of the SNA. Even after one fully loads the particle with negatively charged oligonucleotides, there is still ample room to add more neutral backfill molecules such as PEG. It is noted that the choice of backfill molecule is not just limited to PEG, as a variety of different backfills have also been explored (SI Discussion 1.5 and Figure S12).[4]

CONCLUSIONS

This work is important for the following reasons. First, it provides an important set of design parameters that guide how one should prepare RNA-SNAs for different intended uses. Second, it provides important insight into the unusual structure defined by the SNA and how that structure can accommodate the movement of large macromolecules within it. Third, it uncovers a nonintuitive observation that the spacer motifs, namely, hexaethylene glycol spacer units, dictate the space available to macromolecules. Both the absence of spacer molecules as well as large numbers of spacer molecules leave the most available space for enzymes due to the charged RNA molecules and added flexibility, respectively. Fourth, it is important to consume as much free volume on the nanoparticle surface as possible with ligands, as there is ample room for small, neutrally charged molecules on the nanoparticle surface even after fully loading with RNA. Insights herein on the complex SNA architecture provide a better understanding for how tailored free volume within the SNA and RNA flexibility, enabled by spacer units, can dictate favorable interactions with cellular components such as scavenger receptors, cellular machinery, and proteins. Stability is one part of designing a functional RNA-SNA and future work investigating how stability correlates to other SNA properties such as cellular uptake and gene regulation is ongoing.

EXPERIMENTAL PROCEDURES

Measurement of the Antisense Oligonucleotide Hybridized to the RNA-SNA. To determine the stoichiometry of the AS RNA oligonucleotide to AuNP in a batch of siRNA-SNAs, the concentrations of AS RNA and AuNPs were independently analyzed. To measure siRNA loading on the nanoparticle, Quant-iT Oligreen (Invitrogen) assays against a standard curve were used according to previously established protocols.[14] To start, 3×10^{-12} mol of SNA-siRNA was resuspended in 100 μL of 8 M urea (Sigma-Aldrich) and heated to 45 °C with shaking for 20 min. The solution was diluted with 0.01% Tween-20, to a final concentration of 4 M urea, and centrifuged at 15 000 rpm for 25 min. A portion of the supernatant (25 μL) was analyzed by mixing with Oligreen reagent and measurement of Oligreen fluorescence (λ_{ex} = 480 nm) in a 96 well plate (Biotek synergy plate reader). The concentration of the AuNP was measured by resuspending the pellet in 1 mL of DEPC-treated water and measuring the absorbance at λ_{max} = 520 nm in a Cary-5000 UV−vis spectrophotometer.

Analysis of the Degradation of the AS RNA Oligonucleotide of RNA-SNAs in Media. The lifetime of AS RNA in serum containing media was measured according to previously established methods.[14] SNAs (20 nM in AuNP concentration) were suspended in a solution of 1× PBS or 1× PBS with 10% (v/v) fetal bovine serum (FBS; HyClone) at 37 °C. For reactions in solutions of FBS, an aliquot (150 μL) was removed at time points and mixed with 30 mM sodium dodecyl sulfate (SDS; Sigma-Aldrich) to deactivate serum RNases and stop the reaction. The mixture was then centrifuged at 15 000 rpm for 25 min, at which point the supernatant was removed and the pellet was washed in 0.01% Tween-20 in 1× PBS. After washing, the SNAs were analyzed to determine the ratio of noncovalently associated RNA-oligonucleotide to AuNP (with the protocol described above). The % oligonucleotide remaining was calculated by dividing the AS RNA oligonucleotide per AuNP remaining after specified time in 10% FBS or 1× PBS and dividing it by the AS RNA that was initially hybridized to the AuNP. This ratio is then converted to a percent by multiplying by 100.

Coarse-Grained Molecular Dynamics Simulations (CG-MD). In order to robustly classify the structural properties of the tethered RNA, the gyration tensor S_{ij} was calculated for each tethered RNA strand and its hybridization state (i.e., hybridized or unhybridized) was classified based on whether 50% of the strand was duplexed to the complement strand. The gyration tensor was diagonalized and principal component vectors were tracked. The three calculated eigenvalues can be related to the spherical components of the radii of gyration: $R_G^2(\Theta)$, $R_G^2(\phi)$, and $R_G^2(r)$. Using the R_G components, we calculate the probability distribution $[R_G = [R_G^2(\Theta) + R_G^2(\phi) + R_G^2(r)]^{1/2}]$ of the unhybridized RNA strands for two spacers units: Sp0 and Sp1 for an RNA-SNA with 40% of the RNA duplexed (Figure 3). We calculate the probability distribution ($R_G = [R_G^2(\Theta) + R_G^2(\phi) + R_G^2(r)]^{1/2}$]) of the unhybridized RNA strands for four spacers units: Sp0, Sp1, Sp2, and Sp4 for an RNA-SNA with 40% of the RNA duplexed (Figure S7) and DNA-SNA Sp1 (Figure S9). In order to robustly classify the structural properties of the tethered RNA, the gyration tensor S_{ij} was calculated for each tethered RNA strand and its hybridization state was classified based on whether 50% of the strand was duplexed to the complement strand. The gyration tensor was diagonalized and principal component vectors were tracked.

The coarse-grained RNA bead model parameters that were changed from DNA were the angle bending spring constant and the average H-bond potential per base. This accounted for the increased persistence length that ssRNA has compared to ssDNA as well as the relatively weaker ΔG of hybridization. The stiffness of the ssRNA was increased by 12.5% from 7 to 8 kT/rad^2. The average strength of the H-bond interaction was decreased from 5.5 to 4.35 kT to account for weaker ΔG of hybridization per base in this study.

ASSOCIATED CONTENT

Supporting Information

The Supporting Information is available free of charge on the ACS Publications website at DOI: 10.1021/acs.bioconjchem.6b00350.

Supplementary discussions, figures, and additional materials and methods for SNA synthesis and characterization as well as serum nuclease experiments with linear RNA (PDF)

AUTHOR INFORMATION

Corresponding Author

*E-mail: chadnano@northwestern.edu. Phone: 847.467.7302.

Notes

The authors declare no competing financial interest.

DOI: 10.1021/acs.bioconjchem.6b00350
Bioconjugate Chem. 2016, 27, 2124−2131

■ ACKNOWLEDGMENTS

This material is based upon work supported by AFOSR Award FA9550-11-1-0275, Department of Defense National Security Science and Engineering Faculty Fellowship award N00014-15-1-0043, the Alliance for Cancer Gene Therapy, the NTU-NU Institute for NanoMedicine located at the International Institute for Nanotechnology, Northwestern University, USA and the Nanyang Technological University, Singapore. Research reported in this publication was also supported by the National Cancer Institute of the National Institute of Health Awards U54 CA151880 and U54CA199091; the content is solely the responsibility of the authors and does not necessarily represent the official views of the National Institutes of Health. SNB acknowledges a National Science Foundation Graduate Research Fellowship and a P.E.O. scholar award. A.B.C. acknowledges a National Defense and Science Engineering Graduate fellowship.

■ REFERENCES

(1) Mirkin, C. A., Letsinger, R. L., Mucic, R. C., and Storhoff, J. J. (1996) A DNA-based method for rationally assembling nanoparticles into macroscopic materials. *Nature 382*, 607−609.

(2) Massich, M. D., Giljohann, D. A., Seferos, D. S., Ludlow, L. E., Horvath, C. M., and Mirkin, C. A. (2009) Regulating Immune Response Using Polyvalent Nucleic Acid−Gold Nanoparticle Conjugates. *Mol. Pharmaceutics 6*, 1934−1940.

(3) Massich, M. D., Giljohann, D. A., Schmucker, A. L., Patel, P. C., and Mirkin, C. A. (2010) Cellular Response of Polyvalent Oligonucleotide−Gold Nanoparticle Conjugates. *ACS Nano 4*, 5641−5646.

(4) Barnaby, S. N., Sita, T. L., Petrosko, S. H., Stegh, A. H., and Mirkin, C. A. (2015) Therapeutic Applications of Spherical Nucleic Acids, in *Nanotechnology-Based Precision Tools for the Detection and Treatment of Cancer* (Mirkin, A. C., Meade, J. T., Petrosko, H. S., and Stegh, H. A., Eds.) pp 23−50, Springer International Publishing, Cham.

(5) Seferos, D. S., Giljohann, D. A., Hill, H. D., Prigodich, A. E., and Mirkin, C. A. (2007) Nano-Flares: Probes for Transfection and mRNA Detection in Living Cells. *J. Am. Chem. Soc. 129*, 15477−15479.

(6) Zheng, J., Zhu, G., Li, Y., Li, C., You, M., Chen, T., Song, E., Yang, R., and Tan, W. (2013) A Spherical Nucleic Acid Platform Based on Self-Assembled DNA Biopolymer for High-Performance Cancer Therapy. *ACS Nano 7*, 6545−6554.

(7) Reed, A. N., Putman, T., Sullivan, C., and Jin, L. (2015) Application of a nanoflare probe specific to a latency associated transcript for isolation of KHV latently infected cells. *Virus Res. 208*, 129−135.

(8) Burnett, J. C., and Rossi, J. J. (2012) RNA-Based Therapeutics: Current Progress and Future Prospects. *Chem. Biol. 19*, 60−71.

(9) Burnett, J. C., Rossi, J. J., and Tiemann, K. (2011) Current progress of siRNA/shRNA therapeutics in clinical trials. *Biotechnol. J. 6*, 1130−1146.

(10) Jensen, S. A., Day, E. S., Ko, C. H., Hurley, L. A., Luciano, J. P., Kouri, F. M., Merkel, T. J., Luthi, A. J., Patel, P. C., Cutler, J. I., et al. (2013) Spherical Nucleic Acid Nanoparticle Conjugates as an RNAi-Based Therapy for Glioblastoma. *Sci. Transl. Med. 5*, 209ra152.

(11) Randeria, P. S., Seeger, M. A., Wang, X.-Q., Wilson, H., Shipp, D., Mirkin, C. A., and Paller, A. S. (2015) siRNA-based spherical nucleic acids reverse impaired wound healing in diabetic mice by ganglioside GM3 synthase knockdown. *Proc. Natl. Acad. Sci. U. S. A. 112*, 5573−5578.

(12) Patel, P. C., Giljohann, D. A., Daniel, W. L., Zheng, D., Prigodich, A. E., and Mirkin, C. A. (2010) Scavenger Receptors Mediate Cellular Uptake of Polyvalent Oligonucleotide-Functionalized Gold Nanoparticles. *Bioconjugate Chem. 21*, 2250−2256.

(13) Choi, C. H. J., Hao, L., Narayan, S. P., Auyeung, E., and Mirkin, C. A. (2013) Mechanism for the endocytosis of spherical nucleic acid nanoparticle conjugates. *Proc. Natl. Acad. Sci. U. S. A. 110*, 7625−7630.

(14) Barnaby, S. N., Lee, A., and Mirkin, C. A. (2014) Probing the inherent stability of siRNA immobilized on nanoparticle constructs. *Proc. Natl. Acad. Sci. U. S. A. 111*, 9739−44.

(15) Giljohann, D. A., Seferos, D. S., Prigodich, A. E., Patel, P. C., and Mirkin, C. A. (2009) Gene Regulation with Polyvalent siRNA−Nanoparticle Conjugates. *J. Am. Chem. Soc. 131*, 2072−2073.

(16) Seferos, D. S., Prigodich, A. E., Giljohann, D. A., Patel, P. C., and Mirkin, C. A. (2009) Polyvalent DNA Nanoparticle Conjugates Stabilize Nucleic Acids. *Nano Lett. 9*, 308−311.

(17) Rosi, N. L., Giljohann, D. A., Thaxton, C. S., Lytton-Jean, A. K. R., Han, M. S., and Mirkin, C. A. (2006) Oligonucleotide-Modified Gold Nanoparticles for Intracellular Gene Regulation. *Science 312*, 1027−1030.

(18) Whitehead, K. A., Langer, R., and Anderson, D. G. (2010) Knocking down barriers: advances in siRNA delivery. *Nat. Rev. Drug Discovery 9*, 412−412.

(19) Schroeder, A., Levins, C. G., Cortez, C., Langer, R., and Anderson, D. G. (2010) Lipid-based nanotherapeutics for siRNA delivery. *J. Intern. Med. 267*, 9−21.

(20) Kanasty, R. L., Whitehead, K. A., Vegas, A. J., and Anderson, D. G. (2012) Action and Reaction: The Biological Response to siRNA and Its Delivery Vehicles. *Mol. Ther. 20*, 513−524.

(21) Giljohann, D. A., Seferos, D. S., Patel, P. C., Millstone, J. E., Rosi, N. L., and Mirkin, C. A. (2007) Oligonucleotide loading determines cellular uptake of DNA-modified gold nanoparticles. *Nano Lett. 7*, 3818−21.

(22) Chinen, A. B., Guan, C. M., and Mirkin, C. A. (2014) Spherical Nucleic Acid Nanoparticle Conjugates Enhance G-Quadruplex Formation and Increase Serum Protein Interactions. *Angew. Chem., Int. Ed. 54*, 527−531.

(23) Shim, M. S., and Kwon, Y. J. (2009) Controlled cytoplasmic and nuclear localization of plasmid DNA and siRNA by differentially tailored polyethylenimine. *J. Controlled Release 133*, 206−213.

(24) Schlegel, A., Bigey, P., Dhotel, H., Scherman, D., and Escriou, V. (2013) Reduced in vitro and in vivo toxicity of siRNA-lipoplexes with addition of polyglutamate. *J. Controlled Release 165*, 1−8.

(25) Sato, A., Choi, S. W., Hirai, M., Yamayoshi, A., Moriyama, R., Yamano, T., Takagi, M., Kano, A., Shimamoto, A., and Maruyama, A. (2007) Polymer brush-stabilized polyplex for a siRNA carrier with long circulatory half-life. *J. Controlled Release 122*, 209−216.

(26) Felgner, J. H., Kumar, R., Sridhar, C. N., Wheeler, C. J., Tsai, Y. J., Border, R., Ramsey, P., Martin, M., and Felgner, P. L. (1994) Enhanced gene delivery and mechanism studies with a novel series of cationic lipid formulations. *J. Biol. Chem. 269*, 2550−2561.

(27) Bramsen, J. B., Laursen, M. B., Nielsen, A. F., Hansen, T. B., Bus, C., Langkjær, N., Babu, B. R., Højland, T., Abramov, M., Van Aerschot, A., et al. (2009) A large-scale chemical modification screen identifies design rules to generate siRNAs with high activity, high stability and low toxicity. *Nucleic Acids Res. 37*, 2867−2881.

(28) Raines, R. T. (1998) Ribonuclease A. *Chem. Rev. 98*, 1045−1066.

(29) Haupenthal, J., Baehr, C., Kiermayer, S., Zeuzem, S., and Piiper, A. (2006) Inhibition of RNAse A family enzymes prevents degradation and loss of silencing activity of siRNAs in serum. *Biochem. Pharmacol. 71*, 702−710.

(30) Hong, J., Huang, Y., Li, J., Yi, F., Zheng, J., Huang, H., Wei, N., Shan, Y., An, M., Zhang, H., Ji, J., Zhang, P., Xi, Z., Du, Q., and Liang, Z. (2010) Comprehensive analysis of sequence-specific stability of siRNA. *FASEB J. 24*, 4844−55.

(31) Turner, J. J., Jones, S. W., Moschos, S. A., Lindsay, M. A., and Gait, M. J. (2007) MALDI-TOF mass spectral analysis of siRNA degradation in serum confirms an RNAse A-like activity. *Mol. BioSyst. 3*, 43−50.

(32) Zheng, D., Giljohann, D. A., Chen, D. L., Massich, M. D., Wang, X. Q., Iordanov, H., Mirkin, C. A., and Paller, A. S. (2012) Topical

DOI: 10.1021/acs.bioconjchem.6b00350
Bioconjugate Chem. 2016, 27, 2124−2131

delivery of siRNA-based spherical nucleic acid nanoparticle conjugates for gene regulation. *Proc. Natl. Acad. Sci. U. S. A. 109*, 11975−80.
(33) Cutler, J. I., Auyeung, E., and Mirkin, C. A. (2012) Spherical Nucleic Acids. *J. Am. Chem. Soc. 134*, 1376−1391.
(34) Volkov, A. A., Kruglova, N. S., Meschaninova, M. I., Venyaminova, A. G., Zenkova, M. A., Vlassov, V. V., and Chernolovskaya, E. L. (2009) Selective Protection of Nuclease-Sensitive Sites in siRNA Prolongs Silencing Effect. *Oligonucleotides 19*, 191−202.
(35) Hurst, S. J., Lytton-Jean, A. K., and Mirkin, C. A. (2006) Maximizing DNA loading on a range of gold nanoparticle sizes. *Anal. Chem. 78*, 8313−8.
(36) Senesi, A. J., Eichelsdoerfer, D. J., Brown, K. A., Lee, B., Auyeung, E., Choi, C. H. J., Macfarlane, R. J., Young, K. L., and Mirkin, C. A. (2014) Oligonucleotide Flexibility Dictates Crystal Quality in DNA-Programmable Nanoparticle Superlattices. *Adv. Mater. 26*, 7235−7240.
(37) Sita, T. L. K., F, M., Merkel, T. J., Hurley, L. A., Chalastanis, A., May, J. L., Cayton, T. C., Barnaby, S. N., Savalia, N., James, C. D., Lee, A., Mirkin, C. A., and Stegh, A. H. Dual bioluminescence and near-infrared fluorescence monitoring to evaluate gene regulatory activity of Spherical Nucleic Acid nanoconjugates in vivo, under revision.
(38) Randeria, P. S., Jones, M. R., Kohlstedt, K. L., Banga, R. J., Olvera de la Cruz, M., Schatz, G. C., and Mirkin, C. A. (2015) What Controls the Hybridization Thermodynamics of Spherical Nucleic Acids? *J. Am. Chem. Soc. 137*, 3486−3489.
(39) Daoud, M., and Cotton, J. P. (1982) Star shaped polymers: a model for the conformation and its concentration dependence. *J. Phys. (Paris) 43*, 531−538.
(40) Kohlstedt, K. L., Olvera de la Cruz, M., and Schatz, G. C. (2013) Controlling Orientational Order in 1-D Assemblies of Multivalent Triangular Prisms. *J. Phys. Chem. Lett. 4*, 203−208.
(41) Fankuchen, I. (1941) An X-Ray and Crystallographic Study of Ribonuclease. *J. Gen. Physiol. 24*, 315−6.
(42) Andreatta, D., Sen, S., Pérez Lustres, J. L., Kovalenko, S. A., Ernsting, N. P., Murphy, C. J., Coleman, R. S., and Berg, M. A. (2006) Ultrafast Dynamics in DNA: "Fraying" at the End of the Helix. *J. Am. Chem. Soc. 128*, 6885−6892.
(43) Dormán, G., and Prestwich, G. D. (2000) Using photolabile ligands in drug discovery and development. *Trends Biotechnol. 18*, 64−77.
(44) Masson, C., Garinot, M., Mignet, N., Wetzer, B., Mailhe, P., Scherman, D., and Bessodes, M. (2004) pH-sensitive PEG lipids containing orthoester linkers: new potential tools for nonviral gene delivery. *J. Controlled Release 99*, 423−434.

DOI: 10.1021/acs.bioconjchem.6b00350
Bioconjugate Chem. 2016, 27, 2124−2131